

This document was produced
by scanning the original publication.

Ce document est le produit d'une
numérisation par balayage
de la publication originale.

CANADA

DEPARTMENT OF ENERGY, MINES AND RESOURCES

MINES BRANCH

OTTAWA

Mines Branch Investigation Report IR 72-18

A STUDY OF THE INFRA-RED ABSORPTION IN THE OXIDATION
OF MAGNETITE TO MAGHEMITE AND HEMATITE

by

D. M. Farrell

Mineral Sciences Division

Copy No.

June 29, 1972

Mines Branch Investigation Report IR 72-18
A STUDY OF THE INFRA-RED ABSORPTION IN THE OXIDATION
OF MAGNETITE TO MAGHEMITE AND HEMATITE

by

D. M. Farrell*

- - -

SUMMARY OF RESULTS

Factors affecting the oxidation of magnetite to maghemite and hematite were studied. These included particle size and the presence of water vapour. Infra-red absorption peaks were assigned for the three synthetic minerals, and an unsuccessful attempt was made to calculate the activation energies of the magnetite-to-maghemite and the maghemite-to-hematite reactions. Magnetite appears to oxidize to maghemite via a short-lived "hydroxo" intermediate. Neither the oxidation of magnetite to maghemite nor the crystallographic conversion of maghemite to hematite appear to be simple first- or second-order reactions.

*Chemist, Mineral Sciences Division, Mines Branch, Department of Energy, Mines and Resources, Ottawa, Canada.

CONTENTS

	<u>Page</u>
Summary of Results	i
Introduction	1
Experimental Procedures	2
1. General Considerations	2
2. Sample Preparation	3
3. Sample Testing and Analyses	7
Results and Discussion	10
1. Methods of Preparation	10
2. Difficulties Encountered in Assigning Infra-Red Absorptions	14
3. Analysis of Observed Infra-Red Spectra	21
4. Assignment of Observed Infra-Red Absorptions	26
5. Infra-Red Determination of Water	33
6. Unsuccessful Attempt to Estimate Activation Energies	35
Conclusions	41
Acknowledgements	42
References	43

TABLES

<u>No.</u>	<u>Page</u>
1. Reduction Parameters for Mapico Black	6
2. Infra-Red Spectra of Reduced Mapico Black (RMB) #5 and its Products Formed at 3°C/min Temperature Elevation in Flowing Dry Air	19
3. Infra-Red Spectra of Reduced Mapico Black (RMB) #5 and its Products Formed at 3°C/min Temperature Elevation in Flowing Wet Air	20
4. Computed Bond-Scan Data for Magnetite, Maghemite, and Hematite	31
5. Infra-Red Absorption Peak Observations and Assignments for the Products of RMB #5 Oxidized in Dry and Wet Air	38

FIGURES

<u>No.</u>		<u>Page</u>
1.	DTA of RMB #5 in Flowing Argon, Wet Air, and Dry Air	13
2.	Infra-Red Absorption Spectra of RMB #5 and Its Dry Air Oxidation Products at Selected Temperatures	17
3.	Infra-Red Absorption Spectra of RMB #5 and Its Wet Air Oxidation Products at Selected Temperatures	18
4.	Comparison of Spectral Features at Various Temperatures in the Wet and Dry Oxidation of RMB #5	24
5.	Resolved Spectrum of the 325°C Wet Oxidation Product of RMB #5	39

INTRODUCTION

Magnetite or ferrosferric oxide, Fe_3O_4 , and its metastable oxidation product, maghemite or $\gamma\text{-Fe}_2\text{O}_3$, are crystallographically isomorphous, both having the cubic, inverse-spinel type of crystal structure. Upon heating, $\gamma\text{-Fe}_2\text{O}_3$ undergoes an irreversible transition in structure to hexagonal $\alpha\text{-Fe}_2\text{O}_3$, or hematite, thus completing the process of transformation among the three iron oxides.

The characteristic spinel structure has a cation:anion, metal:oxygen ratio 0.75:1.00, whereas the ratio for the γ -oxide is considerably smaller, \times 0.67:1.00. The generally accepted structure of $\gamma\text{-Fe}_2\text{O}_3$, proposed independently by Hägg⁽¹⁾ and Verwey⁽²⁾, is thus a defect structure in which the unit cell consists of $\text{Fe}_{21.33} \Delta_{2.67} \text{O}_{32.00}$, in which the 2.67 cation vacancies Δ are distributed statistically over the 24 possible cation positions. The filling of the cation vacancies by H_2O has been postulated by several workers. Braun⁽³⁾ has postulated ordering of the $\gamma\text{-Fe}_2\text{O}_3$ spinel structure through the incorporation of water molecules to the limiting hydrogen ferrite spinel of formula $\text{H}_4\text{Fe}_{20}\text{O}_{32}$ (combination) or by combining the accepted oxide $\text{Fe}_{21.33}\Delta_{2.67}\text{O}_{32}$ with H_2O ⁽⁴⁾. The necessity for water in the formation of $\gamma\text{-Fe}_2\text{O}_3$ is shown from the work of David and Welch⁽⁵⁾ and of Sinha and Sinha⁽⁶⁾, who assumed that hydrogen is incorporated as an anion, i. e., as $(\text{OH})^-$ replacing O^{2-} .

The method of infra-red absorption analysis, in conjunction with differential thermal analysis (DTA), thermogravimetric analysis (TGA), and X-ray diffraction (XRD) theoretically appeared to be excellent for determining the exact role of water in the magnetite-to-hematite transformation and for evaluating the semi-quantitative activation energies of the reacting species. This paper is the result of such an investigation as well as a coincident examination of the effects of variables such as grain size and method of preparation of the starting material, magnetite.

EXPERIMENTAL PROCEDURES

1. General Considerations

The oxidation of Fe_3O_4 to $\gamma\text{-Fe}_2\text{O}_3$ and thence to $\alpha\text{-Fe}_2\text{O}_3$ involves 2 distinct reaction processes⁽⁷⁾;

(a) $\text{Fe}_3\text{O}_4 \rightarrow \gamma\text{-Fe}_2\text{O}_3$: This is a topotatic process in which accord between the initial and resultant lattices in three dimensions occurs. Both magnetite and maghemite have the cubic close-packed oxygen sublattices with the inverse spinel structure.

(b) $\gamma\text{-Fe}_2\text{O}_3 \rightarrow \alpha\text{-Fe}_2\text{O}_3$: This is an epitaxial process in which accord between the initial and resultant lattices occurs in two dimensions. $\alpha\text{-Fe}_2\text{O}_3$ has a hexagonal close-packed oxygen sublattice with ferric ions filling 2/3 of the octahedral positions between successive oxygen layers. The ordering of layers shifts from abcabc in maghemite to ababab in hematite.

Feitknecht⁽⁸⁾ has extensively investigated the oxidation processes in magnetite. He found that Fe_3O_4 particles with specific surface areas less than $4\text{m}^2/\text{g}$ (approx.), oxidize by a "nucleation mechanism", in which a concentration gradient of iron ions occurs in an outward direction. Nuclei of $\alpha\text{-Fe}_2\text{O}_3$ are formed in a mixed phase which decomposes into $\alpha\text{-Fe}_2\text{O}_3$ and Fe_3O_4 . The remaining Fe_3O_4 is oxidized directly to $\alpha\text{-Fe}_2\text{O}_3$, and the rate-controlling step is the diffusion of iron ions through the oxygen sublattice. The last remnants of Fe_3O_4 are oxidized only at temperatures exceeding 400°C .

However, Fe_3O_4 with a specific surface greater than $4\text{m}^2/\text{g}$ was found to react quite differently. In this case, the oxidation occurs as a continuous, one-phase reaction for which the following mechanism has been proposed: the oxygen molecules absorbed on the surface of the Fe_3O_4 particles are converted to O^{2-} ions by take-up of electrons in the conversion

of ferrous to ferric ions; the O^{2-} ions attach themselves to the outside of the lattice, and this is presumably the rate determining process; the cation vacancies between the O^{2-} ions are filled by an immediate and even redistribution of iron ions within the lattice. Such an oxidation process takes place between 150 and 400°C.

The $\gamma \rightarrow \alpha\text{-Fe}_2\text{O}_3$ conversion occurs as does the $\text{Fe}_3\text{O}_4 \rightarrow \alpha\text{-Fe}_2\text{O}_3$ transformation; that is, it is epitaxial in nature, involving only the shifting of oxygen layers from the abcabc ordering of the cubic close-packed maghemite oxygen layers to the ababab ordering of hexagonally close-packed hematite oxygen layers.

In summary, the reaction mechanism by which Fe_3O_4 is oxidized is strongly determined by particle size and appears to be influenced to a great extent by factors such as water and impurity content and crystal perfection. Water appears to play a part in transferring the iron ions to new lattice sites, and the presence of internal strain and its partial relief by dislocations appears essential to the initiation of topotactic changes which proceed through the transformation of domains.

2. Sample Preparation

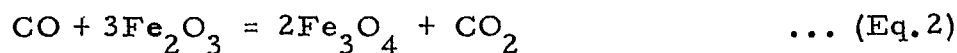
^e Magnetite was synthesized by three methods to determine qualitatively the effects of particle size and/or moisture content.

(a) High-Temperature Reduction of Hematite

Reagent-grade Baker and Adamson α -ferric oxide of 99.00% minimum purity was pelletized at 20,000 lb/in². Principle impurities were: Si 0.10%, Mn 0.06%, Al 0.05%, Mg 0.04%, Ni 0.04%, and Cu and Ti 0.01%, as determined by semi-quantitative spectrochemical analysis. The pellets in zirconium oxide (ZrO_2), furnace boats, were placed at the centre of a horizontal electric cylinder-type furnace. During furnace warm-up, argon was passed through the furnace cylinder over the pellets. The furnace was heated to 1100°C in an argon flow during the warm-up period. The temperature was maintained at 1100°C for 18 hr, during which time the reducing gas

consisting of a 9:1 volume ratio of $\text{CO}_2:\text{H}_2$ was passed through the furnace at approximately 300 cc/min. The furnace was turned off and the reduced hematite was immediately vacuum-desiccated over anhydrous magnesium perchlorate ($\text{Mg}(\text{ClO}_4)_2$) in order to retard decomposition and/or oxidation during cooling.

The reactions occurring during the reduction process at 1100°C were:

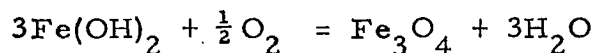
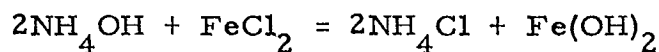


The magnetite was oxidized in both anhydrous and water-vapour saturated air to temperatures of 350, 415, 650, 1050, 1120, and 1200°C , and the oxidation products were analyzed by X-ray diffraction (XRD). The surface areas of the magnetite and the starting material, hematite, were measured by the Brunauer-Emmett-Teller (BET) N_2 absorption method.

(b) Precipitation from Ammoniated Ferrous Chloride Solution

"Baker-Analyzed" hydrated ferrous chloride, $\text{FeCl}_2 \cdot 4\text{H}_2\text{O}$, was dissolved in distilled water and the pH's of the different solutions were brought to 8.5, 11.0, and 12.8 in successive experiments by adding NH_4OH to the sealed reaction flasks. After reaching the desired pH, air was bubbled through a gas dispersion tube into the solution which was agitated by magnetic stirring. For successive runs, the air flow was varied from 1 to 50 ml/min and the flow time from 0.5 to 5.0 hr in 0.5-hr increments. After completion of the reaction, the solvent was decanted, the precipitate was washed thoroughly in air-free 1:1 acetone:water solution and filtered to a paste. The precipitate was then dried under vacuum over $\text{Mg}(\text{ClO}_4)_2$. The entire preparation and separation procedure was performed in a nitrogen atmosphere to avoid extraneous oxidation reactions.

The reactions were:



The specific surface of the precipitate was derived from the BET method.

(c) Reduction of a Magnetite-Goethite Mixture

A sample batch of synthetic precipitated magnetite called "Mapico Black", of quoted 99.0% minimum purity, was obtained from the Columbian Carbon Company, New York, N. Y. Subsequent semi-quantitative spectrochemical analysis revealed the following impurities: Mg 0.1%, Mn 0.09%, Ti 0.007%, and Co 0.02%. However, a determination of ferrous iron, Fe^{2+} , showed only 16.2% Fe^{2+} , whereas stoichiometric Fe_3O_4 or $(\text{FeO} \cdot \text{Fe}_2\text{O}_3)$ should contain 24.1% Fe^{2+} . A preliminary XRD analysis of Mapico Black indicated goethite, $(\alpha\text{-Fe}_2\text{O}_3 \cdot \text{H}_2\text{O})$ as a minor impurity. It was therefore decided to reduce the Mapico Black and bring its Fe^{2+} content to the stoichiometric level.

Five samples of Mapico Black were reduced at moderate temperatures in a $\text{CO}:\text{CO}_2$ atmosphere. ~~The reducing-gas flow was maintained~~ throughout an 18-hr cooling period. The reduced samples (RMB) and their conditions of reduction are listed in Table I. Ferrous iron determinations were made by titration with ceric ammonium nitrate according to Donaldson⁽⁹⁾, whereas total iron (ferrous and ferric) was found by a modified Zimmermann-Reinhardt process, titrating with potassium dichromate ($\text{K}_2\text{Cr}_2\text{O}_7$). Surface determinations were made on the Mapico Black and of RMB 1, 2, 4, and 5 by use of a Perkin-Elmer Sorptometer 212-D and the Brunauer-Emmett-Teller method. The surface areas are also presented in Table I.

After the reduction reactions and the cooling of the oven, the samples were then vacuum-desiccated over $\text{Mg}(\text{ClO}_4)_2$, and RMB #5 was chosen, from the surface area and XRD measurements, as the best product for further experimentation.

TABLE 1

Reduction Parameters for Mapico Black

	Mapico Black (MB)	RMB #1	RMB #2	RMB #3	RMB #4	RMB #5
Reduction Temp. (°C)	-	800	800	800	800	400
Reducing Gas (CO/CO ₂) (V%)	-	9.2/90.8	9.2/90.8	9.2/90.8	10/6/89.4	10.6/89.4
Flow Rate (l/min)	-	0.5	0.75	0.50	1.0	2.0
Reduction Time (hr)	-	6	8	12	8	3
Sample Wt (g)	-	12.8413	13.7673	15.8884	12.5599	28.3745
Reduction Wt (g)	-	12.5164	13.3298	15.4361	12.1578	27.6353
Wt Loss (%)	-	2.53±0.28	3.18±0.10	2.84±0.33	3.29±0.11	2.62±0.31
Specific Surface (m ² /g)	10.3	5.2	0.9	-	0.7	6.2
Fe Total (%)	67.29±0.06	71.16±0.06	-	-	71.37±0.05	71.49±0.08
Fe ²⁺ (%)	16.22±0.03	22.63±0.04	-	-	22.95±0.03	22.97±0.04
Fe ³⁺ (%)	51.07±0.09	48.53±0.10	-	-	48.42±0.08	48.52±0.12
Stoichiometric Fe ²⁺ (%)	24.12	24.12	24.12	24.12	24.12	24.12
Stoichiometric Fe ³⁺ (%)	48.24	48.24	48.24	48.24	48.24	48.24

3. Sample Testing and Analyses

Prior to further experimentation, RMB #5 which had been prepared in two 15-g batches was dried for 24 hr in a vacuum oven between 105 and 110°C. The portion not immediately used was stored under vacuum over $\text{Mg}(\text{ClO}_4)_2$ to prevent the adsorption of atmospheric water and the oxidation of the material.

Differential thermal analyses (DTA) were carried out on RMB #5 under constant conditions. Samples, weighing between 0.6 and 0.7 g were analyzed in flowing argon, in wet air produced by bubbling air through an 80°C water bath, and in dry air produced by passing air through calcium chloride (CaCl_2) and copper sulphate (CuSO_4) prior to passage over the sample. The argon was dried in a like manner before admission to the sample chamber.

In each analysis, a palladium sample holder was employed with α -alumina ($\alpha\text{-Al}_2\text{O}_3$) as the reference standard. A temperature increase of 3°C/min was maintained throughout the analyses, as measured by a platinum-rhodium thermocouple around whose junction the sample was lightly tamped. The gas flow-rate was kept as constant as possible between individual analyses.

Following the preliminary DTA smaller samples, weighing between 0.2 and 0.25 g were again subjected to DTA under the above conditions but at different shut-off temperatures. Wet oxidation was achieved at temperatures between 275 and 650°C, and dry oxidation was achieved at temperatures between 234 and 760°C. Upon reaching the desired temperature maxima, the DTA oven was shut off and the samples were air-quenched to room temperature. The XRD patterns of the samples were recorded by means of a 57.3-mm Debye-Scherrer camera using cobalt radiation and iron filters. Exposure time was approximately 4 hours. DTA products obtained below 400°C were vacuum-desiccated prior to diffraction analysis.

Before recording the infra-red spectra of RMB #5 and its oxidation products, the samples, which had agglomerated because of their fineness and heat treatment, were reduced to finer than 5 microns by grinding in an agate mortar under acetone. Particle size was checked by microscopic examination during the grinding process.

In order to minimize light scattering within the mineral-matrix disks from which the infra-red spectra were recorded, it was necessary that the refractive indices of the mineral and the matrix be as identical as possible. For this reason thallos bromide (TlBr) was chosen as the matrix because its refractive index is between 2.4 and 2.8, whereas that of magnetite is 2.42. A second advantage of TlBr was its non-hygroscopic nature which minimized adsorption of extraneous atmospheric moisture during preparation and spectral recording.

Sample disks were composed of 0.25 wt per cent mineral in TlBr to a total disk wt of 250 mg. The matrix-mineral combination was vigorously mixed by vibration on a "Wig-1-bug" for 5 minutes, and the 250-mg mixture was then pressed into 0.5-in-diameter circular disks at 25,000 psig for 5 minutes under vacuum.

The infra-red absorption spectra of the disks were recorded against a 250-mg TlBr reference under the following conditions:

- spectrophotometer - Beckman IR-12 Infra-red;
- Nernst glower current - 0.60 ampere;
- scanning speed - $40 \text{ cm}^{-1}/\text{min}$;
- gain - 3%;
- period - 8 sec;
- single beam/double beam ratio - 1:1;
- ordinate scale - 0 to 1 absorbance;
- frequency range - 200 to $4,000 \text{ cm}^{-1}$; and
- slit width - variable.

The resultant spectral absorption frequencies and the maximum DTA oxidation temperatures to which the samples were subjected are listed in

Tables II and III for the dry and wet oxidation respectively, and the corresponding spectra are featured in Figures II and III.

In order to separate quantitatively the spectral absorption peaks from the neighbouring peaks, a Dupont Peak Resolver 310 was used. Each oscilloscope pattern of the resolver channels was matched with a standard Lorentzian-type absorption curve. Then, by adjustment of the position, height, and width of the individual oscilloscope pattern to the position, height, and width of the consecutive infra-red peaks, the composition of overlapping peaks and shoulders was resolved, and the pattern of each channel was separately recorded on the spectral curve immediately below the "real" curve. An example of such a resolved spectrum is given in Figure V.

The peak heights (intensities) of the resolved spectra, combined with their respective oxidation temperatures, were used as input data for the unsuccessful attempt at calculation of the activation energies of the magnetite-to-maghemite and maghemite-to-hematite reactions. The activation energy is the minimum energy that a molecule must acquire before undergoing a reaction. The arbitrarily chosen baseline was to be the spectral intensity at 800 cm^{-1} , and the precision of the computations was to depend on how closely the minerals obeyed the Beer-Lambert-Bouguer Law which states:

$$A = -\ln \left(\frac{I}{I_0} \right) = b \sum_{n=1}^N a_n c_n, \quad \text{where}$$

A = absorbance or absorption strength,

I_0 = incident intensity,

I = transmitted intensity,

a = absorptivity,

b = path length,

c = concentration, and

N = component number of the system.

If one can assume that the reactants have absorption frequencies that are completely ~~distinct~~ from those of the products, then the course of a reaction may be followed by carefully recording the decrease in intensity or peak height of the fundamental absorption for one particular reactant. If the path length "b" is constant from sample to sample for that particular frequency, measurement of the peak height or intensity will be a direct measure of the concentration of that particular reactant. The rate of disappearance of that reactant can be determined by following the changes in peak height as a function of time.

However, such a simple system was not found in the present study, and lack of knowledge of the absorption coefficients of the minerals involved was an important reason why a determination of the activation energies for the foregoing reactions could not be made. A detailed description of the relevant activation energy equations and the problems associated with their solution will be presented in the Discussion.

RESULTS AND DISCUSSION

1. Methods of Preparation

(a) High-Temperature Reduction of α -Fe₂O₃

The reduced preparation proved to be pure magnetite by XRD analysis. However, subsequent oxidation of the Fe₃O₄ at temperatures between 200 and 1200°C produced no discernible γ -Fe₂O₃ by XRD. The only product of oxidation to 1050°C was a two-phase mixture of α -Fe₂O₃ and Fe₃O₄. The proportion hematite:magnetite increased with rising temperature. Above 1050°C, α -Fe₂O₃ existed as a pure phase.

Surface determinations of the Fe₃O₄ and the starting hematitic material revealed areas of 0.4 and 11.8 m²/g, respectively. The Fe₃O₄

surface thus qualitatively confirms Feitknecht's⁽⁸⁾ particle size reaction mechanism relationships. The effect of water content could not be confirmed because of the ready availability of water produced during the reduction by Reaction 1. Comparison of the behaviour of completely anhydrous Fe_3O_4 was therefore impossible.

Why not use dry CO?

(b) Precipitation from Ammoniated Ferrous Chloride Solution

Two difficulties in the use of this method were that

(i) the Fe_3O_4 was precipitated from an ammoniated aqueous solution from which it was impossible to obtain completely anhydrous magnetite by dehydration at moderate temperatures, and

(ii) as with most precipitation methods, the product had a very large specific surface, about $70 \text{ m}^2/\text{g}$. Such an area made the magnetite extremely susceptible to oxidation while under near-vacuum conditions at room temperature. A discernible colour change from the jet black of magnetite to the reddish brown of maghemite-hematite was noticed after exposure, for only a few minutes, of the magnetite to air at room temperature. In all attempts at precipitation, traces of lepidocrocite ($\text{FeO}(\text{OH})$) goethite, ($\alpha\text{-Fe}_2\text{O}_3 \cdot \text{H}_2\text{O}$) and FeCl_2 were detected by XRD analysis, inhibiting further investigation of the precipitates.

(c) Reduction of a Magnetite-Goethite Mixture

As the Mapico Black used for reduction had been prepared by precipitation, it was expected that it would still contain traces of water of precipitation even after reduction at 400°C . To test this, a thermogravimetric analysis (TGA) was made on RMB #5 to 800°C in a flowing helium atmosphere. A weight loss of 0.47% occurred over this temperature range and this loss was definitely established as water loss by subsequent chromatographic analysis of the condensed liquid. A marked water loss was observed at between 100 and 105°C , after which the loss became barely discernible by TGA. This dehydration effect implies weak hydration of the

magnetite and very little, if any, bonding of hydroxyl groups within the magnetite lattice. In other words, the hydration appears to be in the nature of physical adsorption rather than chemical bonding.

XRD analysis of RMB #1 revealed a magnetite pattern with a unit-crystal cell edge of 8.393 \AA , in close agreement with the accepted value of 8.394 \AA ⁽¹⁰⁾. However, four unidentifiable reflections of weak intensity were observed at $d = 4.47, 2.33, 1.92, \text{ and } 1.37 \text{ \AA}$. These extra reflections were possibly due to back-reflection. DTA treatment at a temperature elevation of $6^\circ\text{C}/\text{min}$ in wet and dry air yielded X-ray powder patterns of $\gamma\text{-Fe}_2\text{O}_3$ with traces of $\alpha\text{-Fe}_2\text{O}_3$. The specific surface of RMB #1 was $5.2 \text{ m}^2/\text{g}$.

or γ/β

The XRD pattern of RMB #2 was that of single-phase magnetite, but DTA to 330°C and 350°C in wet and dry air produced only a two-phase mixture of hematite and magnetite with no trace of maghemite. DTA to 800°C still revealed minor magnetite in hematite. The specific surface of magnetite was measured at $0.9 \text{ m}^2/\text{g}$. According to Feitknecht⁽⁸⁾ magnetite of such an area oxidizes to hematite only.

RMB #3 consisted of two distinct layers, a black upper phase and a brown lower phase. The low cylinder pressure of CO/CO_2 during the reduction made maintenance of a constant flow of gas very difficult. No attempts at analysis were made.

The XRD pattern of RMB #4 was that of single-phase Fe_3O_4 but with two extra reflections at $d = 2.34$ and 1.92 \AA which again may have resulted from back-reflection. Subsequent DTA and XRD showed a conversion directly from Fe_3O_4 to $\alpha\text{-Fe}_2\text{O}_3$ without formation of the metastable intermediate $\gamma\text{-Fe}_2\text{O}_3$. The specific surface of the Fe_3O_4 was $0.7 \text{ m}^2/\text{g}$.

or γ

The XRD analysis of RMB #5 showed it to be single-phase magnetite with a cell edge of 8.389 \AA . Subsequent DT, TG, and XRD analyses indicated its conversion to hematite via the maghemite intermediate. The specific surface of RMB #5 was found to be $6.2 \text{ m}^2/\text{g}$.

The DT analysis of RMB #5 in flowing argon is shown in Figure 1. The only peak developed was the endotherm at 576°C resulting from the Curie point transition of magnetite from ferrimagnetism to paramagnetism. This

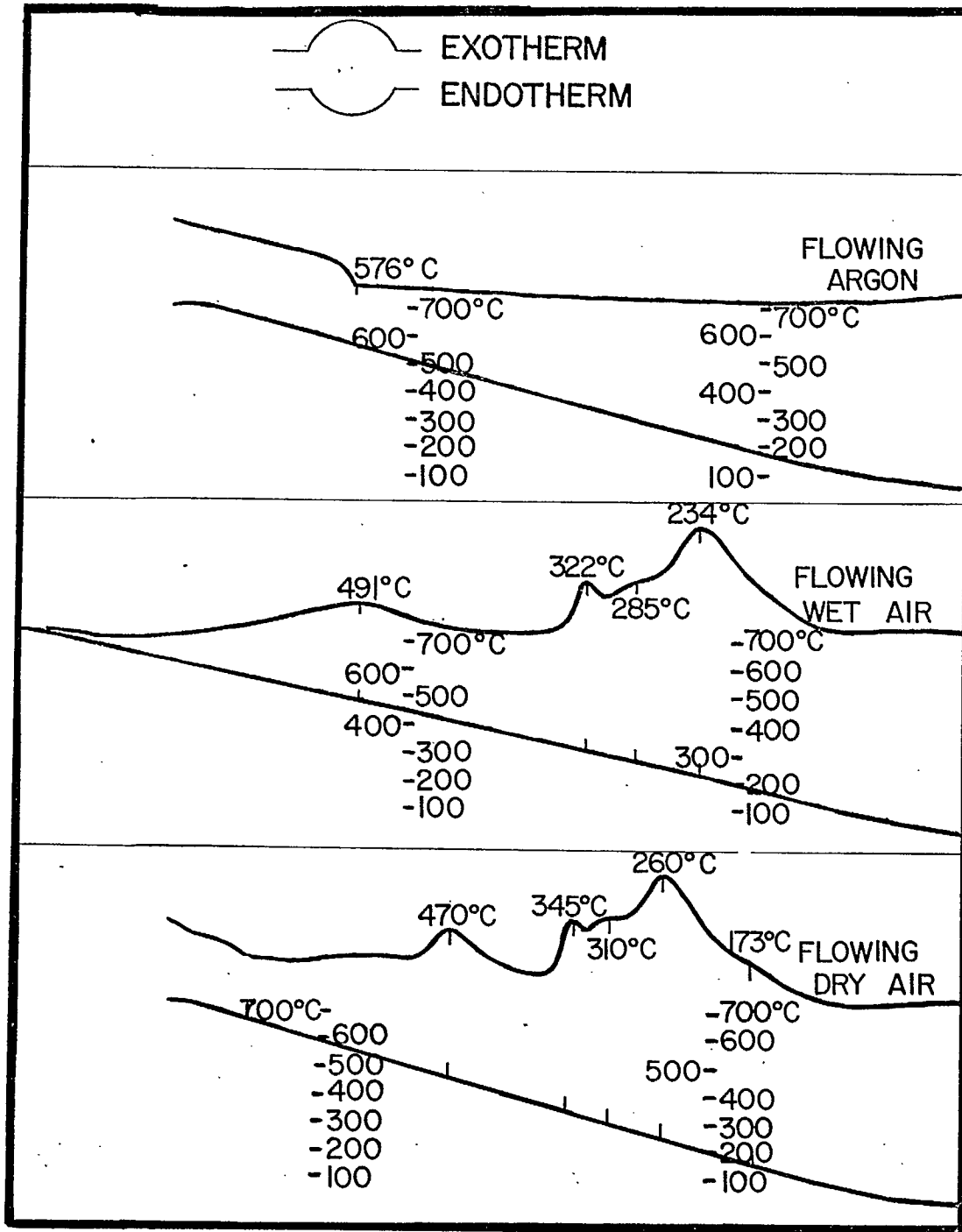


Figure 1. DTA of RMB #5 in Flowing Argon, Wet Air, and Dry Air.

transition temperature is in agreement with that found by Mackenzie⁽¹¹⁾ for synthetic magnetite, the difference in temperature of the endotherm probably being a result of the fine grain size of the magnetite used in the present study.

2. Difficulties Encountered in Assigning Infra-Red Absorptions

Before proceeding to an analysis of the observed infra-red spectra of RMB #5 and its associated oxidation products, a few of the difficulties encountered in making absorption peak assignments will be outlined.

Difficulties such as chemical changes within the sample and chemical reactions between the sample and the medium have been minimized by careful sample preparation, desiccation of the sample to avoid adsorption and oxidation, and by use of TlBr as the medium to avoid sample-medium reaction. However, crystallographic changes within the sample could have occurred during grinding and/or pelletizing. Such changes would generally tend to produce a more disordered structure of higher symmetry, and thereby decreases the number of infra-red absorption peaks observed. The presence of disoriented, fractionated crystals within the infra-red pellets tends to scatter the infra-red radiation so that certain peaks observed may actually be due to refraction rather than absorption. ? fractured?
fragmented?

If one considers the rhombohedral primitive unit cell of the ferrite spinels, $M^{II}Fe_2O_4$, to which both magnetite and maghemite belong, every oxygen anion is bonded to 3 octahedral cations, C_O , and 1 tetrahedral cation, C_T . The three octahedral bonds are mutually perpendicular and provide an isotropic force field in which the oxygen would be free to oscillate in the three directions in the absence of the tetrahedral bond. The tetrahedral cation C_T then introduces a supplementary restoring force along the C_T-O bond, thereby appearing as a stretching vibration of the tetrahedral group. Thus the highest restoring force is directed along the tetrahedral bond and the stretching vibration of the high-frequency absorption peak must thereby be assigned to this bond.

However, in the case of inverse II-III spinels such as magnetite, such an assignment neglects two important factors:

firstly, the effect of strong vibrational interaction between tetrahedral and octahedral subgroups is ignored; provided that such interactions are of sufficient strength to produce either pseudo-octahedral or pseudo-tetrahedral groups, then the vibrations cannot be assigned to either definite subgroup, but instead are related to complex vibrations of the entire spinel lattice⁽¹²⁾;

secondly, even if such interactions are ignored, the proposed assignment will be true only if the C_T-O bond is stronger than the C_O-O bond because the strength of the bond for a given co-ordination number is most strongly dependent on the valency of the cation forming that bond. In the case of magnetite, ferrous ions, Fe^{2+} , occupy only octahedral sites while ferric ions, Fe^{3+} , occupy both octahedral and tetrahedral sites. Therefore, in the case of the inverse spinel on the basis of valency distribution alone, the bond strengths and the consequent vibrational assignments of the octahedral and tetrahedral groups cannot be as clearly defined as in the normal spinel.

From the foregoing discussion, frequency assignments associated with magnetite and maghemite should not be related to specific co-ordination groups, but to complex vibrations of larger groups such as the entire spinel unit cell. Excellent discussions of the interpretations of spinel vibrations are given in papers by Preudhomme and Tarte⁽¹²⁾ and Tarte and Preudhomme⁽¹³⁾.

In general, infra-red vibrational spectra assignments should not be made on the basis of powder data alone. Most workers feel that oriented single-crystal absorption and reflection data ^{are} also necessary in order to make unqualified assignments. However, because of the effect of crystal-size on the magnetite-maghemite conversion, it was not possible in the present study to perform single-crystal investigations. Oriented single crystals minimize the effects of light scattering and lattice distortion outlined earlier.



Roman numerals used earlier

Before proceeding to a detailed discussion of the infra-red absorption spectra of RMB #5 and its oxidation products in dry and wet air, as shown in Figures 2 and 3 and Tables 2 and 3, respectively, some general observations may be made.

The spectra of both dry- and wet-oxidation products, after heating to approximately 500°C, are rather diffuse and the peaks are ~~as~~ asymmetrical. This characteristic is a function of several variables among which are the variation in scatter of the infra-red beam by the small range of particle sizes, the numerous orientations of the crystal fragments within the infra-red pellet, and the differences in refractive index between the mineral component and the matrix material. The latter is known as the Christiansen effect, and occurs because the refractive index of a material is a function of frequency and has a discontinuity in each frequency region of a strong absorption peak, resulting in a distortion of peak shape if there are many large particles. This is the main reason for grinding of the sample and medium to a finer size than the wavelength region of absorption. However, as discussed earlier, the grinding leads to lattice distortion which, in turn, produces weak peaks that may occur in the frequency region of a fundamental and cause further distortion of that peak.

Referring now to Tables 2 and 3 for the dry and wet oxidation of RMB #5, respectively, maghemite exists in solid solution, to varying degrees, with magnetite and/or forms a two-phase mixture with hematite. Under such conditions, it becomes difficult to make definite infra-red vibrational assignments since maghemite is not the sole phase present and the other two phases have similar frequency ranges of absorption. However, by careful discrimination of peak heights variations and XRD analyses, one can formulate tentative assignments. Such assignments will be attempted after a careful analysis of the infra-red spectral peaks for the dry and wet oxidation products has been made.

Figure 2. Infra-Red Absorption Spectra of RMB #5 and its Dry Air Oxidation Products at Selected Temperatures.

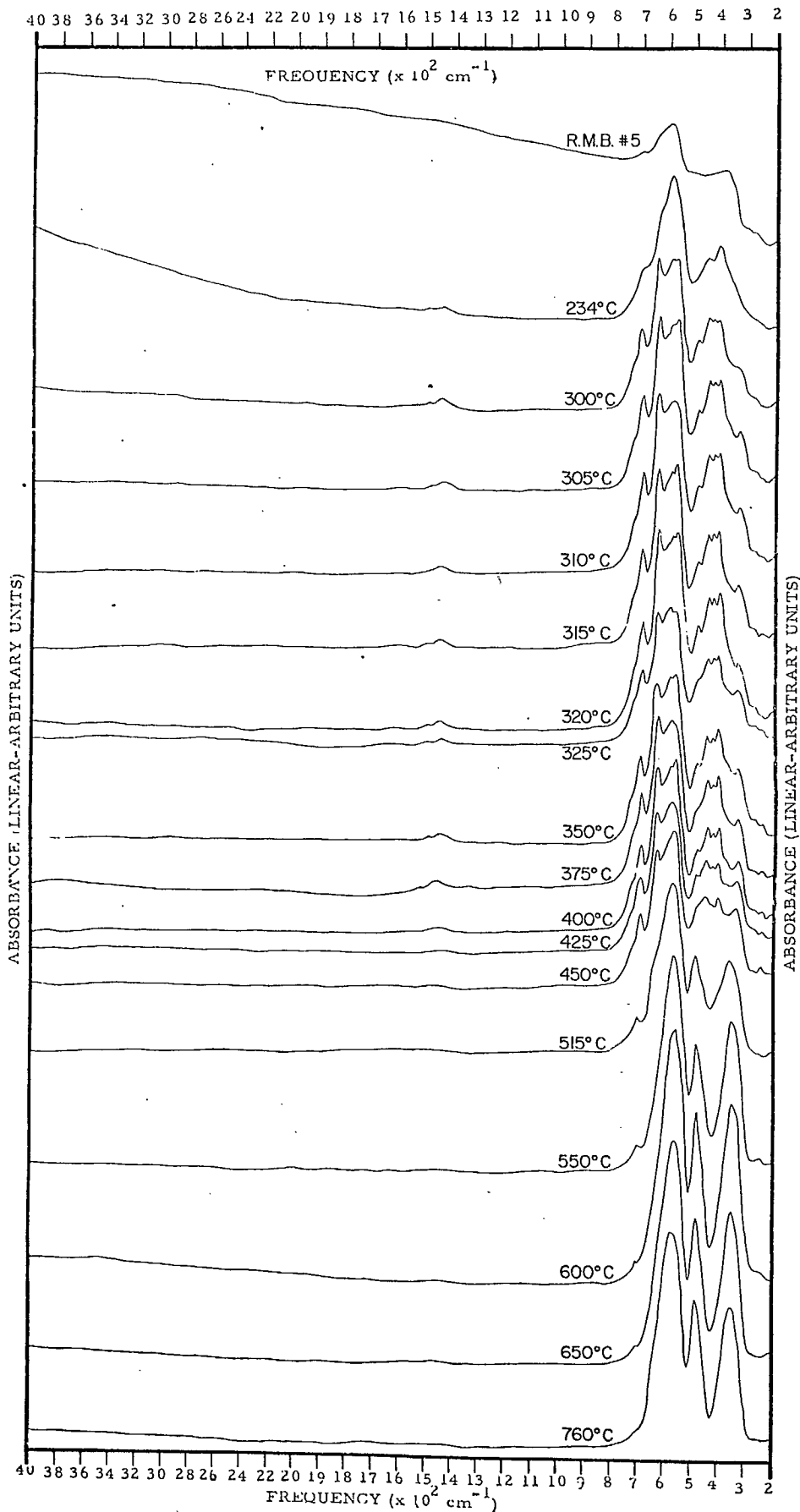


Figure 3. Infra-Red Absorption Spectra of RMB #5 and its Wet Air Oxidation Products at Selected Temperatures.

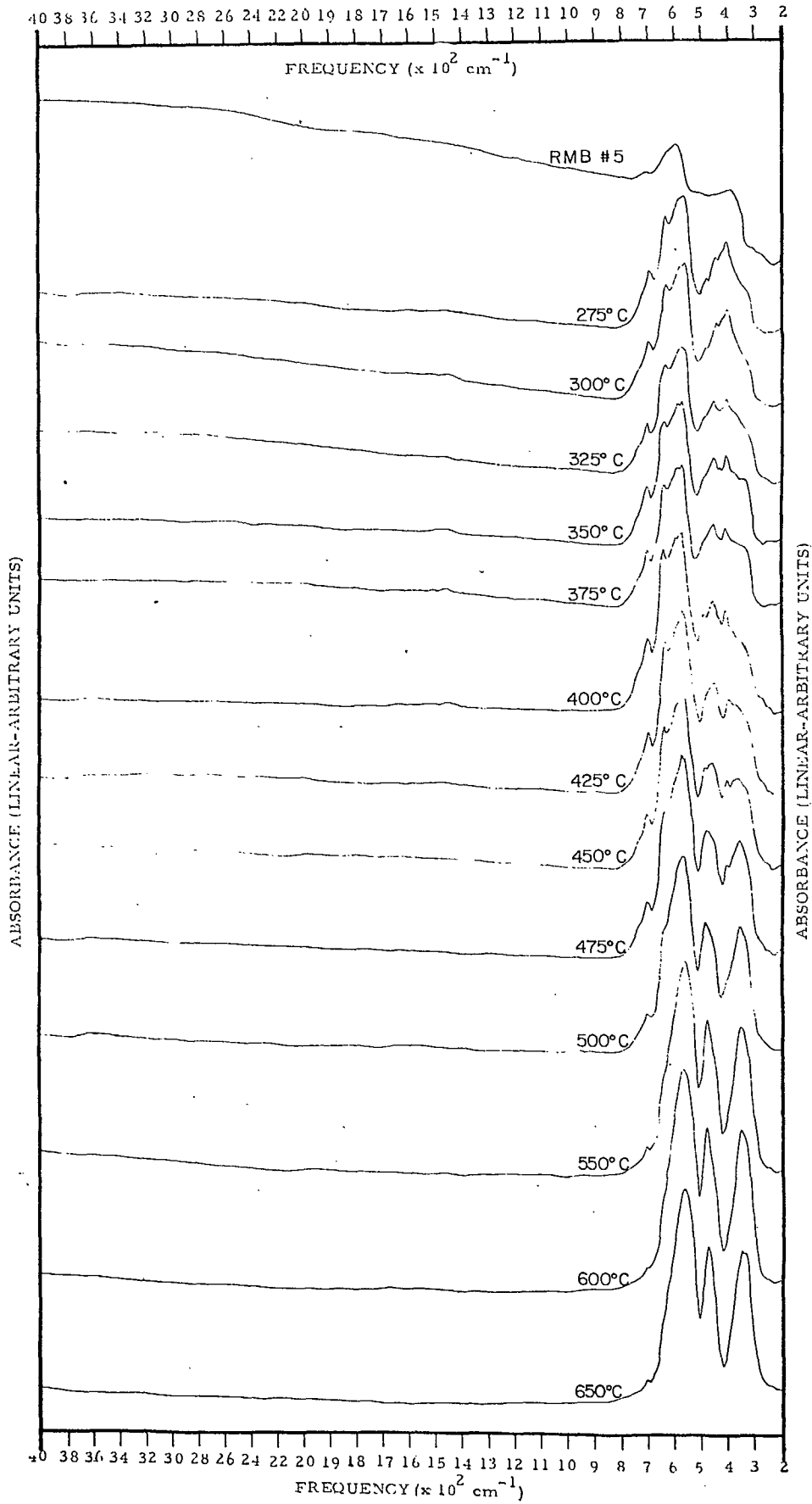


TABLE 2

Infra-Red Spectra of Reduced Mapico Black (RMB) #5 and its Products Formed at 3°C/min Temperature Elevation in Flowing Dry Air

(Figures in Frequency Columns Denote Peak Height from Baseline)

(sh = shoulder)

Sample	Absorption Frequencies (cm ⁻¹)											XRD Analysis
	320	345	400	420	450	480	570	590	630	700	1450	(a = unit cell edge)
RMB #5			26					51		sh18		Magnetite only (a = 8.389 Å)
234°C			28		sh24			54		sh20	3	Magnetite + minor maghemite
300°C	sh18		33	34	35	sh27	57	57	58	32	3	Maghemite + minor magnetite
305°C	24		44	43	44	sh32	67	sh64	68	38	3	Maghemite (a = 8.333 Å) + very small trace (hematite and magnetite)
310°C	27		48	47	47	sh35	67	67	70	40	4	Maghemite (a = 8.337 Å) + very small trace (hematite and magnetite)
315°C	27		47	46	46	sh35	73	70	71	40	4	Maghemite (a = 8.331 Å) + very small trace (hematite and magnetite)
320°C	27		55	53	53	sh42	78	76	79	43	4	Maghemite (a = 8.349 Å) + small minor hematite
325°C	23		36	35	35	sh27	53	55	53	31	3	Maghemite (a = 8.352 Å) + small minor hematite
350°C	28		43	39	40	sh30	64	63	61	33	2	Maghemite (a = 8.343 Å) + small minor hematite
375°C	28		44	41	43	sh32	64	65	66	38	2	Maghemite (a = 8.339 Å) + small minor hematite
400°C	30		42	41	43	sh34	69	sh65	65	36	3	Maghemite (a = 8.351 Å) + small minor hematite
425°C	29		36	34	37	sh31	59		56	30	1	Maghemite + small minor hematite
450°C	32		37	sh34	37	sh34	62		55	30	2	Maghemite + minor hematite
515°C		36					38	66			15	Hematite + minor maghemite
550°C		60					51	85			sh12	Hematite + minor maghemite
600°C		72					69	100			sh11	Hematite + large trace maghemite
650°C		61					58	87			sh 9	Hematite only (a _{hex} = 5.031 Å)
760°C		56					60	85			sh 9	Hematite only (a _{hex} = 5.031 Å)

TABLE 3

Infra-Red Spectra of Reduced Mapico Black (RMB) #5 and its Products Formed at 3°C/min Temperature Elevation in Flowing Wet Air

(Figures in Frequency Columns Denote Peak Heights from Baseline)

(sh = shoulder)

Sample	Absorption Frequencies (cm ⁻¹)											XRD Analysis
	320	345	400	420	450	480	570	590	630	700	1450	
RMB #5			26					51		sh18		Magnetite only (a = 8.389 Å)
275°C	sh16		34	sh30	27	sh19	50	sh49	42	23	2	Maghemite + minor magnetite
300°C	sh18		35	sh31	30	sh20	53	sh48	43	24	2	Maghemite + minor magnetite
325°C	sh19		29	sh25	29	sh22	49	sh48	42	20	6	Maghemite + minor hematite + small trace magnetite
350°C	sh26		34	sh29	33	sh26	55	55	47	22	6	Maghemite (a = 8.321 Å) + minor hematite
375°C	sh24		31	sh27	33	sh26	54	54	47	21	6	Maghemite + minor hematite
400°C	sh25		38	sh35	42	sh36	68	sh66	62	27	3	Approximately equal maghemite + hematite
425°C	sh28		36	sh32	42	sh37	69	sh64	58	23	4	Approximately equal maghemite + hematite
450°C	sh30	35	34		40	sh38	68	sh64	54	21		Approximately equal maghemite + hematite
475°C		45	sh35			49	78		sh56	21		Hematite + minor maghemite
500°C		48				50	75		sh54	15		Hematite + minor maghemite
550°C		57				60	83			sh11		Hematite + small minor maghemite
600°C		62				63	86			sh10		Hematite + trace maghemite
650°C		60				62	84			sh10		Hematite only

3. Analysis of Observed Infra-Red Spectra

From Figure 2, the absorption peak at 320 cm^{-1} appears as a shoulder at 300°C and as a definite but relatively low-intensity peak from 305 to 450°C in dry air. (The general trend is to gradually increasing intensity with temperature to a maximum at 450°C) For oxidation of RMB #5 by wet air, (Figure 3), the 320-cm^{-1} peak first appears as a slight shoulder at 275°C , and remains a shoulder to 450°C , again with a maximum intensity at 450°C .

The absorption at 345 cm^{-1} first occurs at 515°C during the dry oxidation and at 450°C during wet oxidation. The peak attains a maximum height at 600°C during dry oxidation and gradually decreases with higher temperatures. However, during wet oxidation, the maximum was reached at 600°C , with a slight decrease at 650°C .

The 400-cm^{-1} peak occurred in RMB #5 and its oxidation products at 450°C in dry air and 475°C in wet air, with intensity maxima at 320 and 400°C , respectively. The peak intensities varied little in the temperature ranges of the maxima.

The same general pattern occurred with the peaks at 420 cm^{-1} . Again the maxima were at 320 and 400°C for the dry and wet oxidations, respectively, but the peaks first appeared at 300 and 275°C , and disappeared at 450 and 425°C , respectively. The peak resulting from wet oxidation appeared only as a shoulder.

Absorption at 450 cm^{-1} occurred during dry oxidation between 234 and 340°C , with maximum peak height at 320°C . The absorption from wet oxidation occurred between 275 and 450°C with the maximum peak height between 400 and 450°C .

The relative intensities of the absorption at 400 , 420 , and 450 cm^{-1} varied irregularly following oxidation of RMB #5 with dry air. Figure 2 shows the appropriate spectra. At 300 , 425 , and 450°C , the height of the 450-cm^{-1} peak was definitely greater than that of the 400-cm^{-1} absorption but at 305 and 310°C the relative intensities of the two peaks were

nearly equal. The 400-cm^{-1} peak definitely predominated in RMB #5 and in its oxidation product at 234°C and between 310 and 400°C . The 420-cm^{-1} peak was generally minor compared to the 400 and 450-cm^{-1} absorptions. Its relative intensity was nearly equal to that of the 400 and 450-cm^{-1} absorptions at 305 and 310°C .

Quite different variations in the three absorptions occurred during wet oxidation. In all cases the 420-cm^{-1} peak occurred as a shoulder of relatively low intensity, whereas the 400-cm^{-1} absorption which predominated at temperatures below 350°C , gradually became relatively less intense, from 375 to 450°C , than the 450-cm^{-1} peak.

The absorption at 480 cm^{-1} was characterized by shouldering from 300 to 450°C , and the appearance of a definite peak from 515 to 760°C for the dry oxidation. Maximum peak intensity occurred at 600°C , although intensities of similar magnitude were observed at 650 and 760 cm^{-1} . For the wet oxidation (Figure 3), shouldering occurred from 275 to 450°C , and definite peaking from 475 to 650°C . Maximum intensity was again observed at $600 \pm 50^\circ\text{C}$.

As may be observed in Figures 2 and 3, quite dissimilar variations occurred in the relative intensities of the absorption peaks observed at 345 and 480 cm^{-1} resulting from dry and wet oxidation, respectively. For dry oxidation, the 480-cm^{-1} peak was relatively more intense than the 345-cm^{-1} peak at 760 and 515°C , while the 345-cm^{-1} absorption was more intense from 550 to 650°C . For wet oxidation, the 485-cm^{-1} absorption was moderately more intense throughout the temperature range from 475 to 650°C .

For both the dry and wet oxidation products, one of the most intense peaks occurred at 570 cm^{-1} . It was the most intense peak observed at dry oxidation temperatures from 375 to 760°C , and was a major peak to a temperature as low as 300°C . The absorption maximum occurred at 600°C . The 570-cm^{-1} absorption peak from wet oxidation was the predominant peak from 275 to 650°C , and again had maximum intensity at 600°C .

Absorption at 590 cm^{-1} was observed in RMB #5 and the dry oxidation products from 234 to 400°C and in the wet oxidation products from 275 to 450°C . The maxima occurred at 320 and 400°C , respectively. The temperature of the absorption maxima for the 590-cm^{-1} peak was influenced by the strong absorption peak at 570 cm^{-1} . This was particularly true in the case of wet oxidation where the 590-cm^{-1} peak at temperatures from 275 to 325°C and 400 to 425°C appeared as a mere shoulder on the intense 570-cm^{-1} peak.

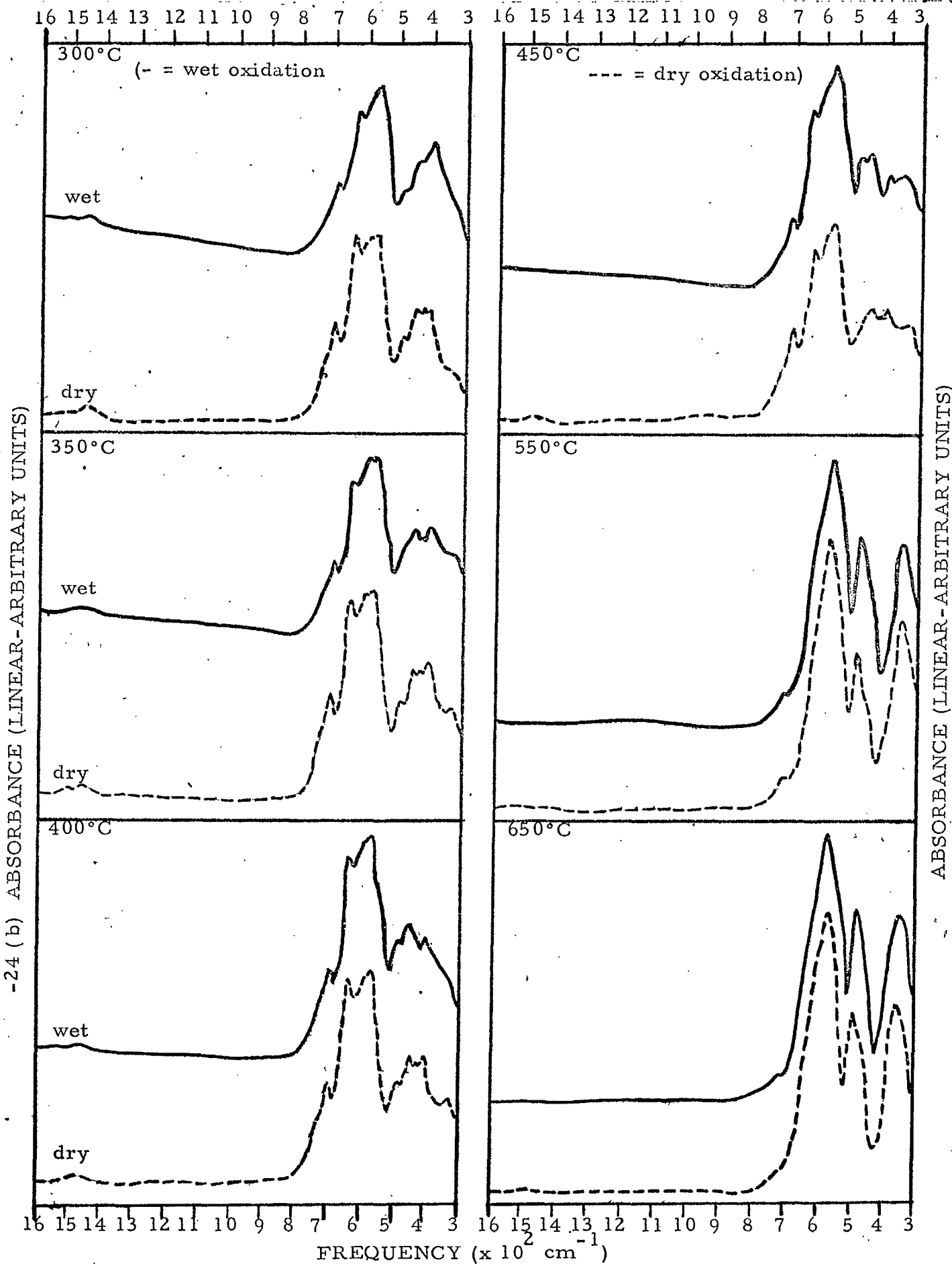
Infra-red absorption at 630 cm^{-1} was observed in the dry oxidation products from 300 to 515°C with maximum peak height occurring at 320°C . The wet oxidation products had similar absorption characteristics at temperatures between 275 and 500°C with the absorption maximum occurring at 400°C .

A comparison of the relative intensities of the absorption peaks at 570, 590, and 630 cm^{-1} for the dry oxidation, Figure 2 and Table 2, shows that the 570-cm^{-1} absorption was clearly the most intense at temperatures exceeding 375°C . However, at temperatures between 305 and 320°C , the 630-cm^{-1} peak was the most intense, while at 325°C the 590-cm^{-1} absorption predominated. The intensities of the three peaks were about equal at 300°C . Except at 325°C , the intensity of the 590-cm^{-1} peak was generally weaker than the other two absorptions. The 570-cm^{-1} peak was not observed at temperatures less than 300°C .

For wet oxidation, quite a different situation occurred. In this case, the 570-cm^{-1} absorption first occurred at 275°C . In the temperature range from 275 to 500°C , the relative peak heights were $570\text{ cm}^{-1} > 590\text{ cm}^{-1} > 630\text{ cm}^{-1}$. The 590-cm^{-1} absorption was generally only a shoulder over its temperature range of observation, room temperature to 450°C . The 590-cm^{-1} shoulder occurred at temperatures 50°C higher than dry oxidation.

The similarities and differences between the spectra of the wet and dry oxidation products can best be observed by reference to Figure 4, in which the spectral region from 300 to 1600 cm^{-1} is shown. The solid-line spectra at the top of the diagrams represent the infra-red absorption result from wet oxidation, while the hatched-line spectra immediately below

Figure 4. Comparison of Spectral Features at Various Temperatures in the Wet and Dry Oxidation of RMB #5.



-24 (b) ABSORBANCE (LINEAR-ARBITRARY UNITS)

ABSORBANCE (LINEAR-ARBITRARY UNITS)

FREQUENCY ($\times 10^2 \text{ cm}^{-1}$)

represent dry oxidation. Oxidation temperatures of 300, 350, 400, 450, 550, and 650°C were chosen for comparison.

Again referring to Figures and Tables 2 and 3, a relatively low-intensity absorption existed at 700 cm^{-1} through the entire temperature range of dry and wet oxidation. Indeed, a weak shoulder was observed at this frequency in RMB #5 itself, so it did not appear to result solely from oxidation. The highest intensity of the peak was observed at 320 and 400°C in the dry and wet oxidation products, respectively.

The highest-frequency peak observed in the spectra was at 1450 cm^{-1} . It occurred in the temperature ranges from 234 to 450°C and from 275 to 425°C during the dry and wet oxidations, respectively. The peak was broad and weak at all temperatures. In fact, if it had occurred in the absorption region of a strong peak, it would likely have been undetected.

In summary, the spectra of the dry and wet oxidation products were generally very similar. The number and frequencies of absorption peaks were identical in the same temperature ranges of oxidation; ten peaks at low and medium temperatures and four peaks at high temperature. The 570 cm^{-1} absorption was generally the major peak at all temperatures in both the wet and dry components. At temperatures over 450°C, the 345- and 480- cm^{-1} absorptions were quite intense, though considerably less than the 570-cm^{-1} peak.

Closer examination of the wet and dry spectral analyses permits observation of definite differences between the two resultant spectral groups. During wet oxidation, maximum peak heights were generally attained at equal or greater temperatures than for dry oxidation. Also, the relative variations in peak height between subgroups of spectral peaks, such as those at 400, 420, and 450 cm^{-1} , those at 345 and 480 cm^{-1} , and those at 570, 590, and 630 cm^{-1} , were markedly different in the dry- and wet-oxidation spectra. As earlier stated, these differences are more readily observed by examination of Figure 4.

4. Assignment of Observed Infra-Red Absorptions

In discussing the infra-red absorption spectra of magnetite and its oxidation products, one is confined to considerations of two basic vibrational modes. One is the stretching vibration, ν , of the Fe-O bonds in the mineral lattices, and the other is the bending, or deformation, δ , of the angle between 3 atoms O-Fe-O, or, equivalently, Fe-O-Fe, where Fe and O are the "anchor atoms", respectively, around which the bond angle will vary during the vibration. The bond-bending vibrations may be in-plane or out-of-plane of the three atoms involved, and are generally of much less intensity than bond-stretching fundamentals. In fact, the intensity of δ vibrations is approximately equivalent to that of overtone and/or combination peaks which will be assumed absent in the present study.

In reference to Tables and Figures 2 and 3, RMB #5 exhibited two broad absorptions at 590 and 400 cm^{-1} which may be assigned to the stretching vibrations of the Fe-O bonds in magnetite. These may be compared to the peaks found by Waldron⁽¹⁴⁾ at 570, and 370 to 380 cm^{-1} and Hafner⁽¹⁵⁾ at 595, and 368 to 397 cm^{-1} , and assigned to the tetrahedral and octahedral sublattices, respectively. Liese⁽¹⁶⁾ observed two peaks at 570 \pm 5 cm^{-1} and 360 cm^{-1} , while Maekawa and Terada⁽¹⁷⁾ observed one peak only at 566 to 588 cm^{-1} in synthetic magnetite. Of the foregoing peaks, only those of Liese⁽¹⁶⁾ were observed in natural magnetite. A variation of 30 to 40 cm^{-1} occurred between the peak frequencies of individual samples. This variation may have been due to differences in preparative procedures or variations in lattice parameters or impurities.

The shoulder existing at 700 cm^{-1} was probably due to a δ vibration.

One can observe from the spectra in Tables 2 and 3 that the vibrational peaks of RMB #5 are much broader and more poorly defined than those of its oxidation products. In fact, they are Gaussian rather than Lorentzian in nature. This effect may arise from two factors: the relatively poor crystallinity of the magnetite compared to its oxidation products; and that magnetite contains both ferrous and ferric ions in octahedral sites

and ferric ions in tetrahedral sites so that, if one assumes lattice vibrations predominating over specific co-ordination vibrations, the net vibrational effect is one of averaging the Fe-O stretching vibrations for both types of sites and ions. The same reasoning will hold for the bending vibrations δ which are probably superimposed at some frequency within the two main absorption peaks.

XRD analysis of RMB #5 confirmed the existence of pure magnetite with a unit cell edge of 8.389 Å.

In the temperature ranges of 300 to 450°C and 275 to 450°C, for the dry and wet oxidation products, respectively, ten infra-red absorption peaks were observed at 320, 400, 420, 450, 480, 570, 630, 700, and 1450 cm^{-1} . Of these, the peaks at 400, 570, 590, and 630 cm^{-1} were the most intense and will be assumed due to the stretching vibrations ν of the Fe-O bonds. The assignment of the 400- and 590- cm^{-1} peaks to the Fe-O stretch is consistent with their assignment for pure magnetite, since in this temperature range the peaks were intense and a major component was found by XRD analysis to be maghemite which has an inverse spinel crystal structure like magnetite. Based solely on intensity considerations, the 570 and 630 cm^{-1} absorptions should also be those of ν Fe-O.

The relatively weak intensity of the peaks at 320, 420, 450, 700, and 1450 cm^{-1} shall be assumed due to the bending vibrations δ of the O-Fe-O bonds. The differentiation between stretching and bending vibrations is rather difficult because of the interspersions, particularly of the hematite peaks, on the spectral patterns within these temperature ranges, resulting in shouldering of spectral features. Some of the frequencies could possibly be due to the stretching vibrations of the maghemite lattice because of the lower symmetry resulting from ordered vacancies.

Absorption at 480 cm^{-1} was likely due to a stretching vibration in hematite.

The only previously reported infra-red vibrational investigation of maghemite in the spectral region of this study was recorded by Maekawa

and Terada⁽¹⁷⁾ who reported absorptions at 448 and 578 cm^{-1} which they did not attempt to assign.

The DTA curves for dry and wet oxidation of RMB #5 are shown in Figure 1, and the corresponding XRD analyses are listed in Tables 2 and 3, respectively.

In general, the conversion temperatures are much lower than those normally found for magnetite oxidation. The DTA exotherms peaking at 234 and 260°C for the wet and dry oxidations, respectively, result from the $\text{Fe}_3\text{O}_4 \rightarrow \gamma\text{-Fe}_2\text{O}_3$ conversion, as confirmed by XRD analysis.

Mackenzie⁽¹¹⁾ found such an exotherm between 275-375°C for synthetic magnetite, while Gheith⁽¹⁸⁾ found a similar exotherm peaking at 210°C in synthetic magnetite. Both authors attribute these temperature differences to variations in particle size and to the catalytic effect of adsorbed water. The lower temperature of conversion of magnetite to maghemite in the present study confirms the catalytic effect of water, since both the wet and dry oxidations were performed on magnetite of the same grain size. However, the infra-red analysis neither confirms nor denies such a catalytic effect, because water was not found by this method. A more complete discussion of the detection of water by infra-red absorption analysis will be made later.

Again referring to Figure 1 and Tables 2 and 3, the exotherms peaking at 322 and 345°C in the wet and dry oxidations, respectively, are a result of the conversion of maghemite to hematite. At these temperatures, XRD analysis showed $\gamma\text{-Fe}_2\text{O}_3$, minor $\alpha\text{-Fe}_2\text{O}_3$, and a small trace of Fe_3O_4 in the wet product, and $\gamma\text{-Fe}_2\text{O}_3$ and minor $\alpha\text{-Fe}_2\text{O}_3$ in the dry product. These may be compared to the conversion temperatures of 590-650°C as determined by Mackenzie⁽¹¹⁾ and Gheith⁽¹⁸⁾ for synthetic magnetite, and 600 to 1000°C for natural magnetite. These temperature differences are again probably due to effects of grain size and/or water content.

Two rather broad, flat exotherms were present in the wet oxidation at 285 and 491°C, and in the dry oxidation at 310 and 470°C. These were probably due to recrystallization processes resulting in energy release and

increased stability. In the temperature range of the low-temperature exotherms, the XRD patterns were that of maghemite plus minor magnetite, so that the exotherm was likely due to recrystallization of the remnant Fe_3O_4 . From Tables 2 and 3, the XRD patterns for the high-temperature exotherms were that of hematite plus minor magnemite so that the exotherm appears to be due to recrystallization of $\gamma\text{-Fe}_2\text{O}_3$.

From the XRD analyses listed in Tables 2 and 3, it can be seen that the main component of the maghemite-hematite two-phase mixture was hematite at temperatures exceeding 515 and 475°C during dry and wet oxidation, respectively.

At these and higher temperatures the infra-red spectra were characterized by three relatively intense absorptions at 345 , 480 , and 570 cm^{-1} . Of these, the 570- cm^{-1} peak may definitely be assigned to the $\nu_{\text{Fe-O}}$ mode, because it had the greatest intensity.

However, some doubt exists regarding the assignment of the peaks at 345 and 480 cm^{-1} . Since the hexagonal unit cell of hematite contains two distinctly different Fe-O bond distances of 1.941 and 2.119 Å⁽¹⁹⁾, one should therefore expect to observe at least two distinct Fe-O stretching frequencies related to these bonds. If one assumes great interaction between mutually bonded and mutually unbonded atoms, then more than two stretching frequencies may be observed, and either or both of the 345 and 480 cm^{-1} peaks may be due to $\nu_{\text{Fe-O}}$. Both are of sufficient strength to be a result of stretching vibrations.

The weak peak appearing at 700 cm^{-1} was observed only as a slight shoulder and as a result of its low intensity may be assigned to the deformation vibration $\delta_{\text{O-Fe-O}}$.

Again referring to Figure 1 and Tables 2 and 3, hematite was initially formed at 322 and 345°C in wet and dry air, respectively. As the temperature was increased, a greater proportion of the maghemite-hematite two-phase mixture was converted to hematite, until at temperatures of 475 and 515°C, XRD analysis revealed mainly hematite. At a temperature of

650°C, XRD analysis showed hematite only, and the length of the unit cell edge of the wet oxidation product was 5.031 Å, in excellent agreement with that of 5.035 Å found by Blake et al⁽¹⁹⁾. As the temperature was increased to 475 and 515°C for wet and dry oxidation, respectively, the infra-red spectra revealed disappearance of the absorption peaks assigned to maghemite and a corresponding preponderance of the absorptions assigned to hematite. This was in very good agreement with the findings of DT and XRD analyses; indeed, agreement was excellent throughout the entire temperature range of study.

Several infra-red investigations have been made on both natural and synthetic hematite in the spectral region of the present study.

Natural α -Fe₂O₃ from Cumberland, England, and Minnesota, and from an unknown origin have been analysed by infra-red absorption by Liese⁽¹⁶⁾, Hunt et al⁽²⁰⁾, and Mitsubishi et al⁽²¹⁾, respectively. Liese⁽¹⁶⁾ found absorptions at 532, 449, 391, and 312 cm⁻¹, Hunt et al⁽²⁰⁾ at 1418, 980, 813, and 752 cm⁻¹, and Mitsubishi et al⁽²¹⁾ at 571, 476, 444, 385, 323, and 235 cm⁻¹. None of these workers attempted to assign the observed peaks. Again, the wide variance in spectral regions of absorption was likely a result of impurities, matrix interference, or inadequate grinding.

Rao and Rao⁽²²⁾ have examined synthetic hematite by infra-red absorption. They observed absorptions at 560 and 452 cm⁻¹, which they assigned to $\nu_{\text{Fe-O}}$, and less intense peaks at and 287 cm⁻¹ which they tentatively assigned to $\delta_{\text{O-Fe-O}}$.

In summary, the observed absorption peaks and their assignments are enumerated in Table 5. Also listed in Table 5 are the spectral observations of both natural and synthetic samples of magnetite, maghemite, and hematite and their proposed assignments as postulated by other workers.

Because the absorption frequencies of the Fe-O bonds are directly associated with the bond lengths, bond-scan analyses were made of magnetite, maghemite and hematite. The lattice constants and atomic co-ordinates so employed were those of Tombs and Rooksby⁽¹⁰⁾ for magnetite, Ueda and

Hasegawa⁽²³⁾ for maghemite, and Wyckoff⁽²⁴⁾ for hematite. The computed bond lengths and associated valence and co-ordination groups are listed in Table 4.

From the bond-length data of the foregoing Table, one can assume that the 570-cm^{-1} absorption common to both maghemite and hematite results from the stretching vibration $\nu_{\text{Fe-O}}$ of the respective 2.080 and 2.084 Å bonds. These bonds are octahedral in maghemite and tetrahedral in hematite. In other words, as stated earlier, vibrational frequencies cannot be assigned to specific co-ordination groups for these minerals.

On the basis of bond-length considerations alone, and noting the close resemblance of the 2.098 Å bond in magnetite to the 2.080 and 2.084 Å bonds in maghemite and hematite, respectively, one may conclude that the 590-cm^{-1} peak in magnetite is due to the vibration of the 2.098 Å bond.

The spectral absorption patterns of magnetite and hematite were relatively simple, with only three and four respective absorption peaks observed. However, in the mid-temperature region of oxidation, from roughly 300 to 450°C, the spectra became quite complex as a result of admixture in various proportions of at least two of the three phases: magnetite, maghemite, and hematite. At no temperature was there clear evidence of water absorption nor undeniable evidence, based on infra-red analyses alone, for the catalytic effect of water in the conversion processes. In general, the spectral features of the wet and dry oxidation products were very similar save for the relative intensities of certain aforementioned absorption peaks.

The only real discrepancy between the XRD, DT, and infra-red methods of analysis was in regard to water. The DTA indicated evidence of the catalytic effect of water in the magnetite-to-maghemite conversion, but no trace of water was determined by infra-red analysis. A possible explanation of this apparently conflicting data will be presented in the following section.

TABLE 4

Computed Bond-Scan Data for Magnetite, Maghemite, and Hematite

Mineral	Lattice Constant (Å)			Octahedral	Co-Ordination	Tetrahedral	Co-Ordination
		Ref.	Present Study	Fe-O Bond (Å)	Iron Valence	Fe-O Bond (Å)	Iron Valence
Magnetite (Fe_3O_4)	8.394	10	8.389	2.098	$\text{Fe}^{2+} = \text{Fe}^{3+}$	1.817	Fe^{3+}
Maghemite ($\gamma\text{-Fe}_2\text{O}_3$)	8.320	23	8.331-8.352	2.080	Fe^{3+}	1.801	Fe^{3+}
Hematite ($\alpha\text{-Fe}_2\text{O}_3$)	5.035	24	5.031			1.956	Fe^{3+}
Hematite ($\alpha\text{-Fe}_2\text{O}_3$)	5.035	24	5.031			2.084	Fe^{3+}

5. Infra-Red Determination of Water

From Figure 1, the endotherm between 110 and 200°C associated with the release of adsorbed water was absent in the present investigation as a result of pre-drying the RMB #5 at 105°C before the oxidation analyses. The water associated with the conversion dynamics of the wet oxidation should therefore have been provided only by the water-vapour saturated air during the process, although residual adsorbed water was likely present during both the wet and dry analyses.

Water in crystalline species may be classified as either lattice or co-ordinated, with no definite borderline between the two. Lattice water refers to water molecules trapped in the crystal interstices and held by weak hydrogen bonds to the anion or the metal, while co-ordinated water refers to water molecules partially covalent-bonded to the metal.

Lattice water absorbs in the infra-red between 3600 and 3200 cm^{-1} , due to OH stretches, 1630 to 1600 cm^{-1} , due to HOH bonds, and possibly somewhat below 600 cm^{-1} due to ~~vibrational~~ vibrational modes resulting from rotational oscillations of the water molecules and restricted by interactions with neighbouring atoms. 

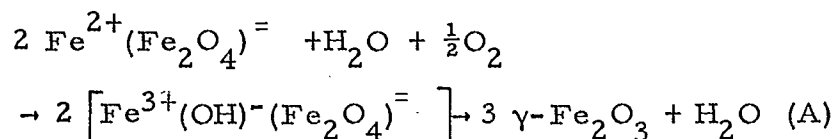
In addition to the three fundamental modes of lattice water, three additional modes will become infra-red-active if the metal-oxygen bond is sufficiently covalent. These are the rocking or in-plane bending vibration, the wagging or out-of-plane bending vibration, and the metal-oxygen stretching vibration of the covalent bond between the cation and the oxygen of the water. In general, such absorptions should all appear below 1000 cm^{-1} and the relative intensities of the stretching and bending vibrations may vary to a great extent depending on the nature of the covalent bond. The greater the covalency, the larger the stretching intensity compared to the bending intensity.

The possibility of forming hydroxo, (OH), complexes must also be considered in the present study. The hydroxo group can readily be distinguished from the co-ordinated-water group because, although each exhibits

the OH stretch between 3600 and 3200 cm^{-1} , the hydroxo complex lacks the HOH bending mode near 1600 cm^{-1} . However, the hydroxo group exhibits the metal-OH bending mode below 1200 cm^{-1} , and can in fact produce a vibration below 700 to 800 cm^{-1} due to hydroxyl bridging. Such bridging has been investigated by Ferraro et al⁽²⁵⁾ in chromium(III) and iron(III) complexes.

It is clear from the foregoing discussion of the infra-red-absorption features of water and its associated hydroxo groupings that there was negligible water or OH content in the oxidation products under discussion. The lack of absorption features from 3600 to 3200 cm^{-1} due to OH stretches, and the similar lack of structure from 1630 to 1600 cm^{-1} , characteristic of HOH bending vibrations, precludes the possibility of the presence of either water or hydroxo groupings. However, the low-temperature DTA exotherm at 322°C, Figure 1, in the wet air oxidation indicates at least a catalytic effect, if not actual adsorption or bonding, resulting from the presence of water. If such a catalytic effect occurs, it must do so either via a short-lived intermediate structure or by a transport mechanism in which water carries oxygen atoms to the reaction sites in the magnetite but does not itself associate with the magnetite lattice.

A possible reaction mechanism for the intermediate type of structure would be:



in which the intermediate is represented by the square bracket. It must instantaneously dissociate to maghemite because a moderately long-lived intermediate would exhibit the normal hydroxo vibrations upon infra-red analysis. The hydroxyl ions in the intermediate would fill the vacancies in the octahedral and tetrahedral interstices of the magnetite lattice. Such a proposed intermediate is in excellent agreement with the postulations of David and Welch⁽⁵⁾ and Sinha and Sinha⁽⁶⁾ regarding the filling of cation vacancies by $(\text{OH})^{-}$ anions with the simultaneous oxidation of ferrous iron to the ferric state.

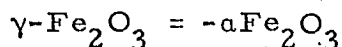
Such a process would likely be a surface phenomenon because the intermediate is apparently short-lived. Such a surface phenomenon would result in the formation of a mixed phase consisting of surface-oxidized magnetite (maghemite) and unoxidized magnetite. Such a mixed phase occurs during wet oxidation at temperatures of 275 and 300°C, Table 3, and during dry oxidation at temperatures of 234 and 300°C, Table 2. However, as stated earlier, residual water was likely present during the dry oxidation, although it was not detected by either DTA or infra-red observations, and this was possibly sufficient to act as a catalyst for the magnetite-to-maghemite conversion, even though no direct evidence existed for the necessity of water in the conversion process.

6. Unsuccessful Attempt to Estimate Activation Energies

As briefly mentioned in Experimental Procedures, Subsection 3, the activation energies for the maghemite-to-hematite and magnetite-to-maghemite reactions, ideally first- and second-order in terms of mineral concentrations, were impossible to compute principally because of lack of knowledge of the absorption coefficients of the relevant minerals. A brief summary of these reactions and their related activation energy equations will be presented here.

(a) First-Order Reaction

A first-order reaction is one in which the reaction rate is directly proportional to the concentration of the reacting species. In the present study, such a reaction could be the conversion of maghemite to hematite:



for such a reaction at a given time t ,

$$k = - \frac{1}{c} \frac{dc}{dt}, \text{ where } k = \text{rate constant}$$

c = concentration of reactant

t = time.

However, in the present investigation, the heating rate during the DT analyses was set at 3°C/min, so that

$$3t = T - 298, \text{ where } T = \text{temperature in } ^\circ\text{K}$$

$$\text{and } dt = \frac{dT}{3}$$

$$\text{so that } k = - \frac{3dc}{cdT} \quad \dots (1)$$

From the Arrhenius Equation:

$$k = Pe^{-E_a/RT} \quad \dots (2)$$

Combining (1) and (2) and integrating:

$$\ln c_1 - \ln c_2 = \ln\left(\frac{c_1}{c_2}\right) = P' \int_{T_1}^{T_2} e^{-E_a/RT} dT$$

where $P, P' = \text{constants}$

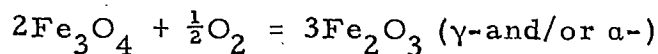
$E_a = \text{activation energy, first-order reaction,}$
in cal/mole

$R = \text{gas constant} = 1.99 \text{ cal/deg mol}$

$c_2, c_1 = \text{concentrations of reactant at temperatures}$
 $T_2, T_1, \text{ respectively}$

(b) Second-Order Reactions

If the reaction rate is proportional to the concentration of two reactants, the reaction is of second order. Such a reaction in the present study could be:



provided that the oxygen was maintained in excess as in the present study.

For such a reaction,

$$k = - \frac{dc}{c^2 dt}$$

again, putting

$$dt = \frac{dT}{3}$$

and employing the Arrhenius Equation,

$$\int_{c_1}^{c_2} \frac{dc}{c^2} = Q \int_{T_1}^{T_2} e^{-E_a/RT} dT, \text{ where } Q = \text{constant}$$

$E_a = \text{activation energy, second-order reaction, in cal /mole}$

$$\text{or, } \frac{1}{c_2} - \frac{1}{c_1} = Q \int_{T_1}^{T_2} e^{-E_a/RT} dT$$

As previously stated, the peak heights of the absorption frequencies of the reactants, as shown in Table 5, were to be assumed directly proportional to the initial and final concentrations c_1 and c_2 , respectively, of the reactants. The peak heights and their corresponding temperatures were then to be incorporated in the activation energy equations previously developed. Figure 5 is an example of a resolved wet oxidation product spectrum.

However, such an assumption regarding the direct proportionality of the peak heights to the concentrations would be true if the reactant under observation was the only one at that specific temperature to vibrate at that specific frequency. In the present study, such was not the case. Rather, the 400 and 590-cm⁻¹ peaks which have been assigned to the fundamental stretching frequencies, ν , of magnetite, are likewise present as fundamentals in maghemite, the oxidation product. Likewise, the 570-cm⁻¹ absorption in maghemite, also absorbs strongly in hematite. Therefore, in order to employ the resolved absorption peak-heights or intensities as reactant concentration parameters, the portion due to the reaction products must be deducted from the total peak intensity. This cannot be done because the absorption coefficients for the minerals are unknown.

Possibly the best choice of frequencies for the activation energy calculation for the maghemite-to-hematite reaction was that at 630 cm⁻¹. This peak was relatively intense within the maghemite temperature region and was observed only with the presence of maghemite. However, this frequency was in close proximity to, and in fact appeared as a shoulder on,

TABLE 5

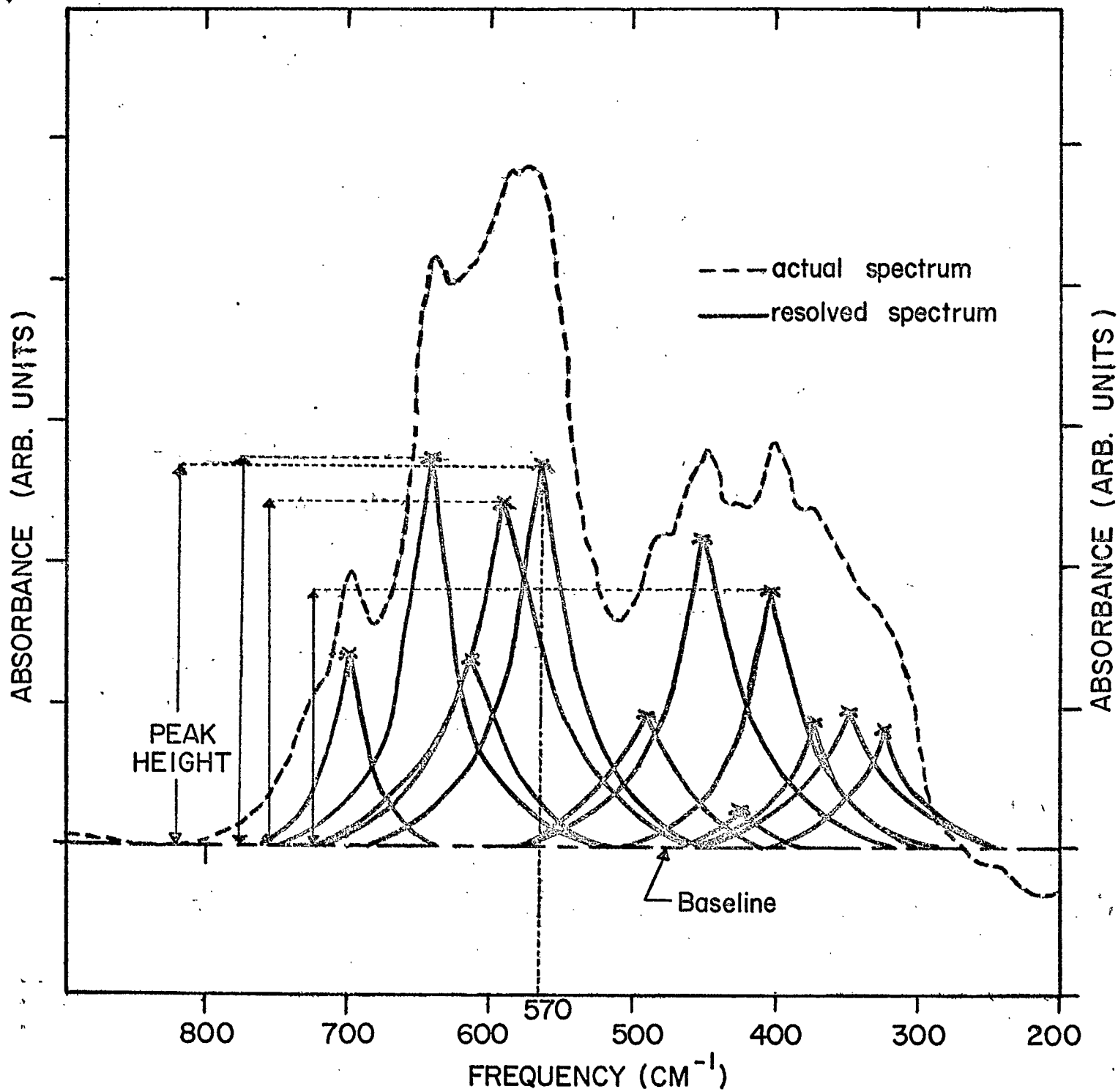
Infra-Red Absorption Peak Observations and Assignments for the Products of RMB #5 Oxidized in Dry and Wet Air

Oxidation Product (from Tables 2 and 3)	Present Study		Reference Investigations									
	Peak (cm ⁻¹)	Assign	Ref 14		Ref 15*		Ref 16	Ref 17*	Ref 20*	Ref 21*	Ref 22	
			Peak (cm ⁻¹)	Assign	Peak (cm ⁻¹)	Assign	Peak (cm ⁻¹)	Peak (cm ⁻¹)	Peak (cm ⁻¹)	Peak (cm ⁻¹)	Peak (cm ⁻¹)	Assign
RMB #5 (Magnetite Fe ₃ O ₄)	590(s,b) 400(m,b) 700(sh)	} ν _{Fe-O} δ _{O-Fe-O}	570 370-380	ν _{Tet Fe-O} ν _{Oct Fe-O}	595 368-397	ν _{Tet Fe-O} ν _{Oct Fe-O}	570 360(w)	588-566 (s, b)				
Maghemite (γ-Fe ₂ O ₃)	400(m) 570(s) 590(s) 630(s) 320(w) 420(m) 450(m) 700(w) 1450(v. w.)	} ν _{Fe-O} δ _{O-Fe-O}						578(s,b) 448(m,b)				
Hematite (α-Fe ₂ O ₃)	570(s) 480(m) 345(m) 700(w)	} ν _{Fe-O} δ _{O-Fe-O}					532 449 391 312	588-556 476-455 333	1418(w) 980(s) 813(w) 752(m)	571 476 444(sh) 385(sh) 323 235	560(s, b) 452(s, b) 396(w, sp) 383(w, sp) 373(w, sp) 345(m, b) 315(m, b) 287(w, b)	} ν _{Fe-O} δ _{O-Fe-O}

Legend

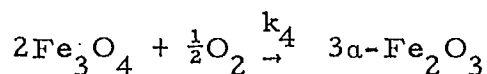
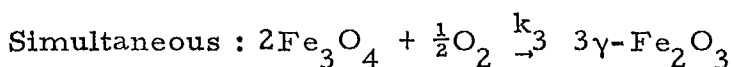
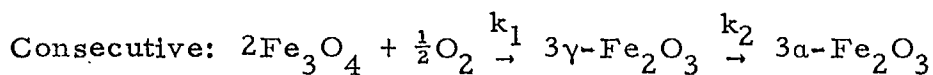
* = wavelength in μ (microns) converted to frequency in wavenumbers (cm⁻¹),
 ν = stretching vibration, δ = bending or deformation vibration,
 Oct = octahedral sublattice, Tet = tetrahedral sublattice, s = strong, m = medium,
 w = weak, v. w. = very weak, b = broad, sp = sharp, sh = shoulder.

Figure 5. Resolved Spectrum of the 325°C Wet Oxidation Product of RMB#5.



the broad, intense 570 and 590-cm⁻¹ peaks, and resolution of the peaks was at best approximate. Further difficulties arose because of the overlapping temperature ranges of stability of the minerals; the simultaneous production of maghemite and enhancement of the 630-cm⁻¹ peak was counteracted by the diminution of the 630-cm⁻¹ peak because of the production of hematite which does not absorb in this spectral region. At no temperature was maghemite the sole phase present so that such interference was probable at all frequencies of absorption.

A major weakness in the computation of activation energies by the preceding method is in the assumption of pure first- and second-order reactions. Instead, probably several reactions are occurring simultaneously. Under the conditions used, competing processes are likely consecutive and/or simultaneous reactions:



The occurrence of these competing processes is evidenced by the occurrence of the three minerals in widely overlapping temperature ranges.

Parameters such as the rate of diffusion of iron ions into the magnetite lattice through surface product layers and the possible, but not proven, catalytic effect of water, should be included in the complete expression of the reaction kinetics. No direct quantitative evidence for such effects was possible in this investigation.

Other problems in the computation of activation energies were physical in nature. Although the infra-red pellets for analysis were very carefully prepared with regard to mineral concentration, the author had great difficulty in obtaining a completely uniform matrix-mineral mixture, so that, in some pellets, opaque aggregations of mineral occurred, to cause increased infra-red absorption.

Considerable difficulty was experienced in resolving the spectra with the Dupont Peak Resolver 310. Theoretically, each change of slope occurring on the shoulders or sides of a peak should be resolved into individual components whose sum equals the unresolved peak. However, in this investigation, the peaks were closely grouped with, at times, considerable shouldering, so that it became impossible to resolve the spectra completely. This was particularly true in the middle temperature range of analysis, where hematite co-existed as a separate phase with magnetite and maghemite.

In summary, the conversion reactions magnetite \rightarrow maghemite \rightarrow hematite do not appear to occur by simple pure first- or second-order processes, but likely involve side reactions and possibly intermediate formation with water to form a hydroxo complex.

CONCLUSIONS

From the foregoing discussion, the following conclusions can be drawn:

1. the temperature of conversion of magnetite to maghemite and hematite appears to be strongly dependent on the magnetite particle size and the presence of water. Maghemite will form if the specific surface of magnetite is $5.2 \text{ m}^2/\text{g}$ but not if it is $0.9 \text{ m}^2/\text{g}$.
2. Maghemite did not appear to form a single phase by itself but was always found in combination with either magnetite or hematite or both. It seems to occur as a surface-layer by-product of oxidation.
3. Oxidation of magnetite to maghemite and conversion of maghemite to hematite occurs at a temperature about 25°C lower in a wet atmosphere than in an anhydrous atmosphere. An hydroxo intermediate may be postulated to explain the reduced temperature of formation of maghemite and its subsequent conversion to hematite.

4. No trace of water or hydroxide was found by infra-red analyses of the mixed maghemite phases, so the proposed hydroxo complex could be a short-lived intermediate.
5. An attempt was made to assign the observed infra-red absorption vibrations of magnetite, maghemite, and hematite to either the stretching or bending modes. Magnetite appeared to have two stretching and one bending mode; maghemite, four stretching and five bending modes; and hematite, three stretching and one bending mode.
6. It was not possible to determine the activation energies for the magnetite-maghemite and maghemite-hematite reactions using fundamental absorption peak intensities because the respective absorption coefficients are not known and because of spectral interference. It appears that the reactions are complex in nature and are neither pure first- nor pure second-order reactions; this supports the supposition of either hydroxo intermediate formation or the occurrence of simultaneous reactions.

ACKNOWLEDGEMENTS

This study was made under the direction of Dr. A.H. Gillieson, Head, Spectrochemistry Section, whose advice and encouragement is gratefully acknowledged.

The TGA and DTA data ^{Wey} was obtained by R.H. Lake, Technical Officer, Physical Chemistry Group; and the XRD analyses were made by E.J. Murray, Technical Officer, Crystal Structure Group. The contributions of these and many other Mineral Sciences Division personnel are accepted with thanks.

REFERENCES

1. G. Hägg, "Die Kristallstruktur des magnetischen ferric oxide, $\gamma\text{-Fe}_2\text{O}_3$ ", Zeits. Krist., B29, 95-103 (1935).
2. E. J. W. Verwey, "The Crystal Structure of $\gamma\text{-Fe}_2\text{O}_3$ and $\gamma\text{-Al}_2\text{O}_3$ ", Zeits. Krist., 91, 65-69 (1935).
3. P. B. Braun, "A Superstructure in Spinel", Nature, 170, 1123 (1952).
4. A. Aharoni et al, "Some Properties of $\gamma\text{-Fe}_2\text{O}_3$ Obtained by Hydrogen Reduction of $\alpha\text{-Fe}_2\text{O}_3$ ", J. Phys. Chem. Solids, 23, 545-554 (1962).
5. I. David and A. J. E. Welch, "The Oxidation of Magnetite and Related Spinel", Trans. Farad. Soc., 52, 1642-1650 (1956).
6. K. P. Sinha and A. P. B. Sinha, "Ein Fehlstellenueberstruktur-Modell für $\gamma\text{-Fe}_2\text{O}_3$ ", Zeits. Anorg. Chem., 293, 228-232 (1957).
7. A. L. Mackay, "Some Aspects of the Topochemistry of the Iron Oxides and Hydroxides", Proc. Int. Symp. React. Solids, 4th, Elsevier, Amsterdam, 571-583 (1961).
8. W. Feitknecht, "The Influence of Particle Size on the Mechanism of Solid Reactions", Pure Appl. Chem., 9, 423-440 (1964).
9. E. M. Donaldson, "Study of Grove's Method for Determination of Ferrous Oxide in Refractory Silicates", Anal. Chem., 41, 501-505 (1969).
10. N. C. Tombs and H. P. Rooksby, "Structure Transition and Antiferromagnetism in Magnetite", Acta Cryst., 4, 474-475 (1951).
11. R. C. Mackenzie, "The Differential Thermal Investigation of Clays", Mineralogical Soc., London, Ch. XII, 299-311 (1957).
12. J. Preudhomme and P. Tarte, "Infra-Red Studies of Spinel - A Critical Discussion of the Actual Interpretations", Spec. Acta, 27A, 961-968 (1971).
13. P. Tarte and J. Preudhomme, "Infra-Red Spectrum and Cation Distribution in Spinel", Acta Cryst., 16, 227 (1963).
14. R. D. Waldron, "Infra-Red Spectra of Ferrites", Phys. Rev. 99, 1727-1735 (1955).
15. S. Hafner, "Ordnung/Unordnung und Ultrarotabsorption IV. Die Absorption einiger Metalloxyde mit Spinellstruktur", Zeits. Krist., 115, 331-358 (1961).

16. H.C. Liese, "An Infra-Red Absorption Analysis of Magnetite", Am. Min., 52, 1198-1205 (1967).
17. T. Maekawa and M. Terada, "Infra-Red Spectrum Study on Corrosion Products of Stainless Steel", J. Jap. Inst. Metals, 29, 421-427 (1965).
18. M.A. Gheith, "Differential Thermal Analysis of Certain Iron Oxides and Oxide Hydrates", Am. J. Sci., 250, 677-695 (1952).
19. R.L. Blake et al, "Refinement of Hematite Crystal Structure", Report of Investigations 7384, U.S. Dept. of the Interior, Bureau of Mines, 1-20 (1970).
20. J.M. Hunt, M.P. Wisherd, and L.C. Bonham, "Infra-Red Absorption Spectra of Minerals and Other Inorganic Compounds", Anal. Chem., 22, 1478-1497 (1950).
21. A. Mitsuishi et al, "Vibrational Spectra of Ruby and Haematite in the Infra-Red Region", Jap. J. Appl. Phys., 1, 1-4 (1962).
22. G.V.S. Rao and C.N.R. Rao, "Infra-Red and Electronic Spectra of Rare Earth Perovskites: Ortho-Chromites, -Manganites and -Ferrites", Appl. Spect., 24, 436-445 (1970).
23. R. Ueda and K. Hasegawa, "Vacancy Distribution in $\gamma\text{-Fe}_2\text{O}_3$ ", J. Phys. Soc. Jap., 17, 391-394 (1962).
24. R.W.G. Wyckoff, "Crystal Structures", published by John Wiley and Sons, New York, 2nd Ed., Vol. 2, 7-8 (1964).
25. J.R. Ferraro, R. Driver, W.R. Walker and W. Wozniak, "Infra-Red Spectra of Several Hydroxy-Bridged Complexes of Chromium(III) and Iron(III) from 650 to 80 cm^{-1} ", Inorg. Chem., 6, 1586-1588 (1967).

DMF/VMcD

= = =